Journal of Physical Oceanography

The DOI for this manuscript is doi:
10.1175/2009JPO4041.1

Wave-driven inner-shelf motions on the Oregon Coast.

Anthony R. Kirincich*

Woods Hole Oceanographic Institution, Woods Hole, MA

Steven J. Lentz

Woods Hole Oceanographic Institution,Woods Hole, MA

John A. Barth

College of Oceanic & Atmospheric Sciences,

Oregon State University, Corvallis, OR

* *Corresponding author address:* Anthony R. Kirincich, Woods Hole Oceanographic Institution, 266 Woods Hole Road, Woods Hole, MA, 02543.

E-mail: akirincich@whoi.edu

ABSTRACT

Recent work by Lentz et al. (2008) documents offshore transport in the inner-shelf due to a wave-driven return flow associated with the Hasselmann wave stress (the Stokes-Coriolis force). We extend their analysis using observations from the central Oregon coast to identify the wave-driven return flow present and quantify the potential bias of wind-driven across-shelf exchange by unresolved wave-driven circulation. Using acoustic Doppler current profiler (ADCP) measurements at six stations, each in water depths of 13-15 m, observed depth-averaged, across-shelf velocities were generally correlated with theoretical estimates of the proposed return flow. During times of minimal wind forcing, across-shelf velocity profiles were vertically sheared, with stronger velocities near the top of the measured portion of the water column, and increased in magnitude with increasing significant wave height, consistent with circulation due to the Hasselmann wave stress. Yet velocity magnitudes and vertical shears were stronger than that predicted by linear wave theory, and more similar to the stratified 'summer' velocity profiles described by Lentz et al. (2008). Additionally, substantial temporal and spatial variability of the wave-driven return flow was found, potentially due to changing wind and wave conditions as well as local bathymetric variability. Despite the wave-driven circulation found, subtracting estimates of the return flow from the observed across-shelf velocity had no significant effect on estimates of the across-shelf exchange due to along-shelf wind forcing at these water depths along the Oregon coast during summer.

1. Introduction

Recent work by Lentz et al. (2008), using 5 years of inner-shelf ADCP observations, found that depth-averaged, across-shelf Eulerian transport was highly anti-correlated with an onshore mass transport due to surface gravity waves. As no net across-shelf transport due to wind forcing would exist in steady conditions along a two-dimensional (2D) coastline, the measured depth-averaged flow is not expected to be correlated with local winds. Yet, the presence of a non-zero offshore transport balancing this onshore mass transport due to waves would lead to a correlation between the depth-averaged, across-shelf velocity and estimates of the Stokes drift. Confirming this hypothesis, the observed vertical structure of across-shelf velocity reported by Lentz et al. (2008) during low winds: offshore, surface intensified, and vertically sheared, was similar to that predicted by wave-driven return flow in the presence of rotation (Hasselmann 1970), especially during the winter unstratified periods. Lentz et al. (2008) used these results as evidence for the importance of wave-driven, across-shelf circulation outside of the surfzone.

That surface gravity waves can force substantial (2-3 cm s^{-1}) sub-tidal, across-shelf velocities in the coastal ocean opens new questions regarding the role of waves in driving inner-shelf, across-shelf transport as well as the potential misinterpretation of wave-driven circulation as wind-driven circulation in previous observations of across-shelf exchange. If present, this wave-driven return flow would be superimposed on across-shelf circulation due to wind or pressure forcing, complicating the analysis of across-shelf exchange observations. In a companion study to Lentz et al. (2008), Fewings et al. (2008) found that wave-driven circulation had a profound effect on observations of across-shelf exchange due to wind forcing,

altering the measured vertical structure of across-shelf velocity during all but the smallest wave climates. A recent study of the inner shelf off the central Oregon coast (Kirincich et al. 2005), which reported a relatively strong across-shelf circulation due to along-shelf wind forcing, might be similarly influenced by this wave-driven return flow.

In this work, we extend the analysis of Lentz et al. (2008) using observations from the central Oregon coast to determine whether a similar wave-driven return flow is present, and to quantify the potential bias of wind-driven circulation due to unresolved wave-driven circulation. The central Oregon inner shelf has distinct differences from the two inner-shelf locations examined by Lentz et al. (2008). Most notably, the Martha's Vineyard and North Carolina shelves examined by Lentz et al. (2008) were offshore of relatively smooth coastlines and adjacent to straight, wide shelves subject to variable wind and buoyancy forcings. In contrast, inner-shelf locations along the Oregon coast are offshore of relatively rocky coastlines and adjacent to a steep, narrow shelf whose dynamics during summer is driven primarily by along-shelf winds (Huyer 1983). At large scales (10s of km), wind and wave forcing as well as bathymetry are along-shelf uniform. Yet, areas inshore of the mooring locations (<13 m water depth) are more heterogeneous with significant small-scale (10s of meters) along-shelf variations (Kirincich et al. 2005).

The important elements of this wave-driven, sub-tidal circulation can be understood by restating the basic theory used by Lentz et al. (2008). On timescales much longer than a wave period, the onshore Stokes transport characteristic of surface gravity waves is written as:

$$U_w = \frac{Q_w}{h} \approx \frac{gH_{sig}^2}{16c} cos(\theta_w) \tag{1}$$

where g is gravitational acceleration, H_{sig} is the significant wave height, c is the phase speed, and θ_w is the incoming wave direction. This transport is defined in the Eulerian sense as an onshore mass transport above the wave troughs (Figure 1A). However, in the Lagrangian sense, the Stokes transport is defined as an onshore-directed, vertically-sheared velocity profile occurring throughout the water column (Figure 1B). Assuming linear wave theory, this Lagrangian Stokes velocity is given as:

$$u_{st}(z) = \frac{H_{sig}^2 \omega k}{16} \frac{cosh(2k[z+h])}{sinh^2(kh)} cos(\theta_w) \tag{2}$$

where ω is the wave frequency in rad s^{-1}, k is the wavenumber in rad m^{-1}, z is the vertical coordinate, and h is the local water depth. If conditions are uniform alongshore (*i.e.* two-dimensional), this onshore transport is offset by an offshore Eulerian transport in order to conserve volume. Within the surfzone, the vertical structure of this offshore 'undertow', parabolic with maximum offshore velocities at mid-depth, is controlled by the vertical gradient of turbulent stress. However, a different balance and vertical structure may exist outside of the surfzone where the Earth's rotation is important. Here, the influence of the Coriolis parameter (f) on the wave orbital velocities drives an along-crest wave stress (τ^w):

$$\frac{\partial \tau^w}{\partial z} = -\rho_o f \frac{H_{sig}^2 \omega k}{16} \frac{cosh(2k[z+h])}{sinh^2(kh)} \tag{3}$$

known as the Hasselmann wave stress (Hasselmann 1970) or the Stokes-Coriolis force (Polton et al. 2005). Combining equations 2 and 3, the vertical gradient of this stress can be written in terms of the theoretical Lagrangian Stokes velocity:

$$\frac{\partial \tau^w}{\partial z} = -\rho_o f u_{st}, \tag{4}$$

and thus we define a theoretical Eulerian 'Hasselmann' velocity (u_H) that is the exact op-

posite of the Lagrangian Stokes velocity (Figure 1):

$$u_H = -u_{st}. \tag{5}$$

If the gradient of the Hasselmann wave stress is balanced by the Coriolis force in the along-crest momentum equation of an open-ocean mixed layer:

$$\rho_o f u_{obs} = \frac{\partial \tau^w}{\partial z} = \rho_o f u_H, \tag{6}$$

the observed (Eulerian) velocity profiles will exactly balance the Stokes (Lagrangian) drift. This balance can occur when the fluid is considered to be inviscid (Ursell 1950), or when the Ekman layer depth is small compared to the Stokes layer depth, the no-wind limit (Polton et al. 2005).

The role of wave drift in a rotating ocean is a topic of ongoing research. Following the identification of the wave-driven Eulerian flow (Ursell 1950; Hasselmann 1970), the effects of waves on surface flows in open-ocean mixed layers were examined through a variety of analytical studies [e.g. Madsen (1978); Weber (1981, 1983)]. Together these works have formed a theoretical description of the interactions between wind stress, wave generation and decay, and surface Ekman currents in deep water. Subsequent work has compared theory to observations (Polton et al. 2005) and developed methods to incorporate wave effects into general ocean circulation models (Perrie et al. 2003; Weber 2003; Rascle et al. 2006). However, much of this work has focused on deep-water waves in open-ocean mixed layers, and often assumed fully-developed seas. Additional complexity may exist in the shallow waters of the inner shelf where the surface and bottom boundary layers overlap and interact, stratification is spatially and temporally variable, and where the wave field feels the effects of the shallow, shoaling bottom. Although recent work exists in this area (Monismith and

Fong 2004; Newberger and Allen 2007; Lentz et al. 2008), the role of wave-driven circulation in these shallow environments deserves further attention. Can the wave-driven return flow be seen as clearly in other locations as it was in Lentz et al. (2008)? Does its presence lead to a misinterpretation of across-shelf exchange due to other processes (*i.e.* wind-forced circulation)?

To attempt to answer these questions, we examined the effects of surface-gravity waves on inner-shelf upwelling circulation using velocity observations from six deployments of acoustic Doppler current profilers (ADCPs) made during the 2005 summer upwelling season along the central Oregon coast. Using this dataset, we find evidence of a similar wave-driven circulation that appears to have little effect on measurements of across-shelf exchange driven by the along-shelf wind. However, nearshore bathymetric variability present in the region causes significant spatial variability that, in concert with the strong temporal variations found, impeds our ability to find results as conclusive as those of Lentz et al. (2008). We proceed by first describing the velocity and wave observations along with the methods used to estimate the wave-driven circulation (Section 2). Results are then presented for the inferred depth-averaged return transport as well as the vertical structure of the low-wind across- and along-shelf velocities (Section 3). The potential influence of the wave-driven circulation on observations of wind-driven circulation is investigated by computing the fraction of full theoretical Ekman transport present within the surface layer, a measure of across-shelf exchange efficiency, while accounting for the wave-driven circulation (Section 4). Finally, we discuss these findings along with their implications for previous and future studies (Section 5) before summarizing our results (Section 6).

2. Data and methods

a. Data sources

From April to September 2005, the Partnership for Interdisciplinary Studies of Coastal Oceans (PISCO) Program maintained four inner-shelf stations (LB, SR, YB, and SH) along a 67 km stretch of the Oregon coast (Figure 2) centered around Newport, Oregon (44.6° N). At each station, all located in 15 m of water, a bottom-mounted upward-looking ADCP was deployed and serviced twice during the field season. The ADCPs, RDI Workhorse 600-kHz units, sampled velocity profiles from 2.7 m above the bottom to 2 m below the surface with 1 m vertical bins; making ensemble averages of 40 pings, using a ping rate of 1.5 s, every 2 minutes. In addition to these four ADCP stations, two deployments of a Nortek 1-MHz Acoustic Wave And Current (AWAC) profiler were made near stations SH and LB in water depths of 15 m (station SHN) and 13 m (station LBS). At station SHN (LBS), the AWAC sampled velocity profiles for 40 minutes of every hour using 2 (3) minute ensemble averages composed of 40 (80) pings, using a ping rate of 1.5 s, and 0.5 (1) m vertical bin spacing. For the remaining 20 minutes of the hour at both stations, the instrument collected bursts of 1-Hz near-surface along-beam velocity (for 3 beams), 2-Hz acoustic surface height (from a center beam), and 1-Hz bottom pressure observations to resolve the directional wave spectrum.

Wind measurements collected at NOAA's Coastal-Marine Automated Network (C-MAN) station NWP03 were used in this analysis. Station NWP03, located on the south jetty of the Newport harbor entrance (Figure 2), is representative of nearshore winds throughout the study area during summer (Kirincich et al. 2005; Samelson et al. 2002). Wind stress was cal-

culated following Large and Pond (1981) assuming neutral stability. Observed winds during the 2005 season (Figure 3) were atypical for the central Oregon coast, oscillating between generally weak upwelling-favorable wind events (negative wind stress) and strong downwelling-favorable wind events until day 195 when strong and persistent upwelling-favorable winds began. Across-shelf winds were strong early in the season, before becoming weak (more typical) as stronger upwelling commenced (Figure 3). The atmospheric causes and oceanic effects of this anomalous wind forcing are detailed in a recent work by Barth et al. (2007).

Significant wave heights and dominant wave periods measured during the AWAC deployments averaged 1-2 m at 6-8 s with numerous peak events reaching 3-5 m at 10-13 s (Figure 3). Directional spectra from the AWAC (not shown here) revealed both simple wave fields having a single peak as well as more complex fields with multiple wave peaks originating from different offshore locations. No reflected waves were detected during the AWAC deployments, despite the rocky nearshore topography at both stations. Incoming peak wave direction was mixed before day 195 but predominantly from north of 'shore-normal' (positive wave direction) after day 195, generally following the wind direction (Figure 3). Significant wave heights (H_{sig}) and wave frequencies (ω) from the AWAC sites were positively correlated (H_{sig}:0.93, ω:0.63) at the 95% confidence interval with those collected 33 km (20 NM) west of Newport by the NOAA NDBC buoy 46050 (located at 44.62° N 124.53° W). Throughout this analysis, 95% confidence intervals and levels of significance were found using the effective degrees of freedom following Chelton (1983). Additionally, wave heights, wave frequencies, and wave directions from the AWAC sites were similarly correlated with observations at NDBC buoy 46089, the nearest buoy recording wave direction (located 110 km NNW of station LBS at 45.91° N 125.76° W). These favorable comparisons indicate that the wave cli-

mate was relatively uniform over the central Oregon shelf during this time. However, waves propagating from the offshore buoys to the AWAC had consistently smaller wave heights at the AWAC (regression slopes of 0.78 for AWAC/46050 and 0.72 for AWAC/46089) and the incoming wave direction was consistently smaller (more 'shore-normal') at the AWAC locations (Figure 3), both expected due to wave refraction and dissipation.

b. Calculation methods

As local wave observations did not exist at all stations or all deployment times, we used the wave conditions measured at buoy 46050 to create timeseries of onshore wave transport (U_w) at each station. Based on the favorable comparisons between the AWAC and buoy observations shown above and in Figure 3, the significant wave height observations from buoy 46050 appear representative of wave conditions throughout the region. However, given the reduction in wave height from the offshore NDBC buoy to the inner-shelf AWAC sites, H_{sig} from buoy 46050 was reduced with a linear transformation, using the slope of 0.78, to more closely match the magnitude of H_{sig} measured in the inner shelf. Additionally, lacking measurements of wave direction at buoy 46050, we simplified (1) by assuming incoming waves were normal to the orientation of the local coastline (θ_w=0), defined by the principal axis of flow at each station as described below. With these simplifications, an estimate of the theoretical depth-averaged offshore return velocity (U_w) was obtained for each station by dividing the onshore wave transport, estimated using the reduced buoy 46050 H_{sig}, by the local, hourly measured, water depth (U_w = -Q_w/h). The phase speed (c) in (1) was calculated from hourly estimates of water depth (h) and wave number (k). The effects of

these simplifications were were assessed through comparisons to the local wave observations at SHN and LBS (see Appendix), which found that using the wave climate at buoy 46050 and assuming θ=0 generally overestimated U_w by 10% or less.

To estimate the observed across-shelf transports and the vertical structure of across-shelf velocities from the moored measurements, hourly-averaged velocity profiles were first interpolated onto a regularly spaced vertical grid and normalized by the hourly water depth to reduce bias due to the 2-m tidal fluctuations (spanning 3 vertical bins at most stations). Profiles were then extrapolated from the measured area of the water column to the surface and bottom using a linear extrapolation of the top two measurements to the surface and a linear interpolation between the bottom-most measurement and zero at the bottom boundary. These full water column velocity profiles were rotated into an along- and across-shelf coordinate system defined by the principal axes of the depth-averaged, subtidal velocities during times of small wave heights ($H_{sig} < 1$ m). This calculation was performed on each instrument sub-deployment separately, to account for possible compass errors. In general, principal axes varied by less than $\pm 3^{\circ}$ at each station, within the accuracy of the instrument compasses, and were aligned along-isobath. A 'west-coast' coordinate system is used here so that offshore (generally westward) is the negative across-shelf direction while upwelling favorable, southward winds are in the negative along-shelf direction. The depth-averaged (U_{obs},V_{obs}) and depth-dependent (u_{obs},v_{obs}) across- and along-shelf velocities were calculated for each station following this method before being low-pass filtered using a 40 hr half power period (Mooers 1968) to isolate the subtidal components of variability.

The extrapolation method described above was chosen because it maximized the correlations between the depth-averaged across-shelf velocity (U_{obs}) and the theoretical return flow

(U_w) at most sites while minimizing correlations between the difference of U_w and U_{obs} (U_{res}) and the across-shelf wind stress. As U_{obs} should be uncorrelated with the winds given the assumption of along-shelf uniformity used here, minimizing the wind-induced component of U_{obs} is critical to isolating the wave-driven across-shelf transport. Additional methods (*e.g.* no extrapolation or velocity 'slab' extrapolations) yielded qualitatively similar results for the wave-driven dynamics, but had depth-averaged residual velocities that were more strongly correlated with the across-shelf wind stress. During circulation driven by across-shelf winds, across-shelf velocity profiles exhibit strong surface intensification, with the zero crossing of the across-shelf velocity profile occurring higher in the water column than during circulation driven by along-shelf winds (Fewings et al. 2008; Tilburg 2003). Extrapolations not accounting for these strong surface flows, which may be poorly resolved by our observations, would have an unbalanced bottom return flow that would bias the depth-averaged mean and lead to a negative correlation between U_{res} and the across-shelf wind stress. Consistent with this idea, using the alternative extrapolation methods led to stronger negative correlations between U_{res} and the across-shelf wind stress at all stations, particularly during the first part of the season when across-shelf winds were larger (Figure 3).

3. Wave-driven circulation

Using the methods described above, we examined velocity observations from the six stations to identify the wave-driven portion of the across-shelf circulation by looking both at the depth-averaged, across-shelf velocity during all times and the depth-dependent velocity during times of minimal wind forcing. These results are presented first, after which we

attempt to account for this wave-driven circulation while re-examining across-shelf exchange driven by along-shelf wind stress.

a. Depth-averaged across-shelf velocity

The observed depth-averaged across-shelf velocities (U_{obs}) at all sites are shown in Figure 2, and correlation coefficients and linear regression slopes between U_{obs} and the theoretical return flow (46050 U_w) are given in Table 1. Combining all data, U_{obs} and U_w were significantly, but not strongly, correlated (cc=0.45) with a regression slope of 0.80±0.22. The total correlation coefficient and regression slope given here for water depths of 15 m were similar to correlation and regression results reported by Lentz et al. (2008). In their study, Lentz et al. (2008) found correlations decreased with increasing water depth from 0.55 to 0.4 in water depths of 12 and 17 m. Regression slopes were similar for both depths at 1±0.3.

Despite mean values equal to that found by Lentz et al. (2008), correlation coefficients and regression slopes varied dramatically between stations as well as over time. Correlation coefficients, taken over the length of each deployment (the *All* column in Table 1), varied from a high of 0.78 at station LBS to a low of 0.32 at station SH. Regression slopes between U_w and U_{obs} also varied between sites, from a high of 2.2±1.32 at LBS to a low of 0.27±0.16 at SH. Comparing individual timeseries of U_{obs} (Figure 2) illustrates the strong differences that existed among the stations and with U_w. Individual period/station correlation coefficients were significant most often during the first period (days 120-150). Marked by a strong wave event from the southwest on days 138-145 (Figure 3), station correlations ranged from 0.39 to 0.75 and slopes ranged from 0.25±0.23 to 1.02±1.05 for this period (Table 1). Time period

results from station YB, most often significant, varied only slightly in correlation coefficients but dramatically in slope, from 0.54±0.35 during days 150-190 to 2.75±2.26 during days 230-270. Slopes much higher than one occurred only after day 190 at stations LBS and YB.

The reasons for these larger regression slopes can be seen visually in Figure 2. At stations YB and LBS, U_{obs} was visually larger than 46050 U_w after day 190, especially near days 210, 240, and 260. In contrast, at stations SH and SR, U_{obs} was characterized by much smaller variations during these time periods, with magnitudes close to that of U_w. Results at LBS and SHN using AWAC U_w, which includes the effect of wave direction, were quantitatively similar to those presented here.

With the 2D assumption used, wind forcing should not contribute strongly to U_{obs}. Thus, the residual across-shelf transports (U_{res}=U_{obs}-U_w) were compared to the local wind forcing to assess how well the wave-driven transport was isolated. With the method of extrapolation chosen, individual station residuals were generally uncorrelated with both the along- and across-shelf wind stresses. Exceptions included a weak negative correlation between SR and across-shelf wind during days 110-150, a weak positive correlation between SH and the along-shelf wind during days 110-150, and a weak positive correlation between YB and the along-shelf wind during days 150-190. For all stations combined, U_{res} was positively correlated with the along-shelf wind stress (cc=0.18) and negatively correlated with the across-shelf wind stress (cc=-0.15), though both correlations were quite weak. This correspondence of the residual to the winds occurred primarily in the first two time periods (before day 190) when across-shelf winds were stronger than normal and along-shelf winds were variable (Figure 3).

More than correlation or regression results, the correspondence between the depth-averaged, across-shelf velocity and the theoretical wave-driven return flow can be illustrated

by bin-averaging the two timeseries by the level of significant wave height. To make this comparison, hourly values of H_{sig}/h from all stations (N=12688) were sorted into ascending order and divided into eight consecutive bins of equal sample size (n=1586). Calculating the mean and standard error of the corresponding hourly values of U_{obs} and U_w for each bin gives a bin-averaged comparison (Figure 4) that is equivalent to Figure 7 of Lentz et al. (2008). For bins with small H_{sig}/h, or small theoretical return flows, the observed depth-averaged velocities were less than the theoretical values (Figure 4) and near zero. As U_w increases, observed velocities become increasing negative, approximately matching the theoretical magnitude for values of U_w greater than 0.005 m s^{-1}. Perhaps driving the differences seen between U_{obs} and U_w at low values of H_{sig}/h, timeseries of U_{obs} at stations LB, SR, and SHN tend to have onshore flows during periods of minimal wave forcing (Figure 2). However, despite the small standard error bounds given for the first few bins, the difference between the two timeseries for these bins was within the absolute accuracy of the instruments themselves. Additionally, the departures from theory shown were not quantitatively different from those of Lentz et al. (2008). As a narrower range of H_{sig}/h was observed at the Oregon stations compared to Lentz et al. (2008), a smaller range of velocities was spanned here with finer resolution.

b. Vertical profiles during low-wind forcing

As described by Lentz et al. (2008), only the vertical structure of the return flow reveals whether it was driven by surfzone processes (volume conservation and wave breaking) or by the effects of rotation on the wave orbital velocities (Hasselmann wave stress). To isolate the vertical structure of the observed across-shelf velocities, the hourly depth-dependent

velocities during times of minimal wind forcing (N=4768, 37% of the total observations), were sorted by the magnitude of the corresponding wave heights (as H_{sig}/h) into four bins of equal sample size (n=1192). Times of minimal wind forcing were defined, following Lentz et al. (2008), as when the absolute wind stress $\mid \vec{\tau}^s \mid$ was less than 0.03 N m^{-2}. Mean across- (u) and along-shelf (v) velocity profiles were estimated for each of these wave height bins.

1) Low-wave, low-wind velocity profiles

The bin-averaged, across-shelf velocity profiles (Figure 5: *left panel*), had an increasingly negative (offshore) velocity structure superimposed on a minimal-wind, minimal-wave velocity profile. The vertical structure of this base profile (assumed here to be the H_{sig}=0.7 m profile) was offshore in the top 4 m, onshore between 11 m *hab* (height above bottom) and 4 m *hab*, and offshore again in the lower portion of the water column. The corresponding minimal-wind, minimal-wave, along-shelf velocity profile was southward with strong vertical shear, approaching 0.06 to 0.05 m s^{-1} near the surface and zero near the bottom of the measured area (Figure 6: *left panel*). Mean wind stress during times of minimal winds ($\mid \vec{\tau}^s \mid < 0.03$ N m^{-2}) was -4.8x10^{-3} N m^{-2}, along-shelf and upwelling favorable. However during times of minimal winds and minimal waves (the H_{sig}=0.7 m bin), along-shelf wind stress was slightly stronger at -6.8x10^{-3} N m^{-2}. Thus the bulk of the across- and along-shelf velocities found for this bin may represent a weak upwelling circulation with southward along-shelf flow, offshore flow above 11 m *hab*, and onshore flow in the middle of the water column.

These base across- and along-shelf velocity profiles were similar to mid-shelf observations reported by Lentz and Trowbridge (2001) for the Northern California coast during winter. In

their work a weak upwelling wind was responsible for the surface and interior flows, while the bottom offshore flow coincided with isopyncals sloping downward towards the coast. Previous analysis of hydrographic measurements at the PISCO stations during weak winds found increased stratification below a 3-4 m thick surface mixed layer (Kirincich and Barth 2009), consistent with the across-shelf velocity structure found here. However, no information about the near-bottom, across-shelf density structure exists at these locations. The limitations of the method used to extrapolate velocity profiles was apparent in the across-shelf profiles as sharp velocity discontinuities occurred at the transition to the bottom interpolation region at 2.5 m *hab*.

2) Wave-driven velocity profiles

Wave-height dependent changes in the vertical structure of the across-shelf velocity were isolated by subtracting the base profile ($u_{0.7}$) from the remaining three bin-averaged velocity profiles. These differenced profiles, of which only the measured portion of the water column is presented in the right panel of Figure 5, appear to represent increases in the wave-driven return flow over the base minimal-wind, minimal-wave profile. Theoretical estimates of these differenced profiles were included in the panel for comparison, calculated for each bin using the bin-averaged significant wave height and dominant wave periods in (2) and (5), assuming θ=0, before subtracting the theoretical base profile. Observed profiles had strong vertical shear with larger velocities near the top of the measured portion of the water column and magnitudes that increase with increasing significant wave height. These characteristics are qualitatively consistent with wave-driven return flow due to the Hasselmann wave stress

(Stokes-Coriolis force). However, the observed profiles were larger in magnitude and had larger vertical shear than the corresponding theoretical profiles (Figure 5). The observed wave-driven profiles also have decreased velocities at the top of the measured portion of the water column, in contrast to the theoretical predictions. Contamination of the surface-most bins of the ADCP is common at higher significant wave heights, potentially causing the reduced velocities seen here. Despite these differences from linear theory, the inferred wave-driven, across-shelf velocity profiles observed here were similar both in magnitude and shear characteristics to the 'summer' profiles described by Lentz et al. (2008) for these water depths.

A similar 'base profile' plus 'wave-driven return flow' decomposition was not found for the bin-averaged, along-shelf velocity profiles. Subtracting $v_{0.7}$ from the higher wave-height profiles resulted in strongly sheared northward velocities for all bins (Figure 6: *right panel*), which is inconsistent with along-shelf circulation forced by the Hasselmann wave stress. As shown by Lentz et al. (2008), model results for the along-shelf velocities due to the Hasselmann wave stress are vertically uniform and reduced in magnitude compared to the corresponding across-shelf velocities. Despite bin-averaging by wave height, non-zero mean along-shelf wind stresses existed for each of the four bins: at -6.8x10^{-3}, -6.0x10^{-3}, -3.0x10^{-3}, and 1.0x10^{-3} N m^{-2} for the H_{sig}= 0.7, 0.9, 1.0, and 1.5 m bins respectively. The magnitudes and vertical structure of the bin-averaged, along-shelf velocities (Figure 6: *left panel*) are consistent with forcing from these bin-averaged, along-shelf wind stresses, perhaps superimposed onto a constant northward pressure gradient. This correspondence between the bin-averaged wind stress and along-shelf velocities, both bin-averaged by wave height, illustrates the difficulties in fully separating the wind-driven and wave-driven dynamics.

4. Effect on observations of wind-driven exchange

In a recent study of inner-shelf, wind-driven circulation at these stations, Kirincich et al. (2005) estimated the fraction of full theoretical Ekman transport present in the observed across-shelf surface transport due to forcing by the along-shelf wind stress. Using data from the 1999-2004 upwelling seasons and without accounting for any potential wave-driven circulation, the authors found an average fraction of 0.25 of full Ekman transport at water depths of 15 m, 1-1.5 km offshore, and full Ekman transport at water depths of 50 m, 5-7 km offshore. Given the recent findings of Fewings et al. (2008) described earlier, the vertical structure of a wave-driven offshore return flow could constructively interfere with across-shelf circulation due to upwelling-favorable winds, perhaps increasing the transport fractions estimated by Kirincich et al. (2005). To determine whether the wave-driven circulation contributed to the amount of wind-driven exchange reported by Kirincich et al. (2005) in 15 m of water, we repeat the analysis using the observed across-shelf velocity profiles of the 2005 dataset and compare the resulting fractions to those calculated for across-shelf velocity profiles modified to account for the wave-driven circulation.

Two estimates of the across-shelf, wave-driven circulation were made. The first was based on the theoretical Hasselmann velocity profiles (u_H) and calculated directly from (5) using hourly observations of wave height, water depth, and wave period. The second estimate was based on the vertical structure of the minimal-wind, bin-averaged velocity profiles (Figure 5) with the minimal-wind, minimal-wave profile ($u_{0.7}$) removed (u_{ap}). For each hour, profiles of u_{ap} were calculated by interpolating the bin-averaged velocity profiles (Figure 5: *right panel*) to a velocity profile corresponding to that hour's significant wave height using a

linear interpolation/extrapolation at each vertical level. u_{ap} may underestimate the vertical structure observed for a given wave height, as the structure for $u_{0.7}$ was removed as part of the background vertical structure.

From the observed across-shelf velocity profiles (u_{obs}), as well as the two differenced estimates (u_{obs}-u_H and u_{obs}-u_{ap}), timeseries of across-shelf surface transport (U_s) were computed by subtracting the depth-averaged mean before integrating from the surface to the first zero crossing, following Kirincich et al. (2005). These estimates of across-shelf surface transport were compared to the theoretical full Ekman transport, based on the along-shelf wind stress ($U_{ek}=\tau_s^y/\rho_o f$), using a neutral regression (Garrett and Petrie 1981; Reed 1992) to find the fraction of full Ekman transport (Table 2) at each station.

Results for the calculation were statistically significant for all profile variations at stations SR, YB, SHN, and SH and for u_{obs}-u_{ap} at station LB. Estimated fractions at these stations ranged from 0.16 to 0.24, within the range of values reported by (Kirincich et al. 2005). While these results were strongly station dependent, at each station there were no significant differences between transport fractions calculated with the full observed across-shelf velocities and those modified to account for an estimate of the wave-driven return flow. We infer from the similarities found among individual station results that the wave-driven Eulerian velocities present in the observations did not significantly affect this bulk calculation used to understand the time-averaged, wind-driven circulation. This was a surprising result given the sizable wave-driven circulation described above (Figure 2 and Table 1). Yet as the depth-averaged mean velocity was removed to compute the across-shelf surface transport, only the vertical structure of the wave-driven circulation alters the Ekman fraction calculation.

Comparing the depth-dependent portion of the three different profile types for the same magnitude of wind forcing (τ_s^y=0.052 N m^{-2}), equivalent to U_{ek}=$\pm$0.5 m^3 s^{-1}, illustrates the small effect the vertical structure of the wave-driven circulation appears to have on wind-driven exchange (Figure 7). For U_{ek}=-0.5 m^3 s^{-1}, corresponding to upwelling-favorable conditions, the differenced profiles were similar in structure and slightly reduced in magnitude relative to the observed profile. For U_{ek}=0.5 m^3 s^{-1}, corresponding to downwelling favorable conditions, the u_{obs}-u_H differenced profile was similar in structure and slightly increased in magnitude relative to the observed profile. However, using the larger wave-driven return flow estimate, u_{ap}, the $u_{obs} - u_{ap}$ profile had onshore velocities in the surface layer that were as much as double u_{obs} (Figure 7). These changes to the differenced profiles were consistent with constructive interference of the wind and wave-driven circulations during upwelling conditions and destructive interference during downwelling conditions. Examining the three profile types for a range of along-shelf wind stresses finds similar results to those shown in Figure 7; only slight differences exist for all wind conditions except moderate to peak downwelling for the the $u_{obs} - u_{ap}$ profile.

Having a number of potential causes, these larger across-shelf velocities in the $u_{obs} - u_{ap}$ profile during downwelling were not frequent enough to effect the time-averaged Ekman fraction calculation. The larger difference between the profiles, compared to upwelling conditions, might be partially due to reduced Ekman transport fractions during downwelling events, shown to occur in both observations (Kirincich and Barth 2009) and model results (Austin and Lentz 2002). Downwelling events along the Oregon coast also tend to have higher significant wave heights for a given theoretical Ekman transport magnitude (Figure 8), increasing the vertical structure of the wave-driven circulation, especially for u_{ap}.

However, moderate to strong downwelling winds occurred far less frequently than upwelling winds, accounting only for 32% of the observations (Figure 8), thus these differences for the $u_{obs} - u_{ap}$ profile during downwelling were unable to significantly bias the mean fraction of full Ekman transport found at any station.

5. Discussion

From the comparisons shown above, it is clear that a portion of the depth-averaged, across-shelf velocities observed on the Oregon inner shelf can be explained by a return flow associated with Lagrangian Stokes drift. Moreover, combining the results for all stations and averaging over different levels of H_{sig}/h appeared to be a successful way to reduce the large amounts of variability found within the timeseries themselves. Only after doing so were we able to attain results equal to those found by Lentz et al. (2008).

The spatial and temporal variability seen in both the correlation coefficients and regression slopes (Figure 2, Table 1) have a number of potential causes. Station locations, sampling durations, methodological choices (*i.e.* extrapolation type, principal axis definition), as well as spatial and temporal variations in the wind and wave climates all may have contributed to the variability seen. As was illustrated by the bin-averaged, along-shelf velocities, the relatively short record lengths impeded our ability to effectively isolate the wave-driven circulation and might have complicated the comparisons of U_w and U_{obs}. However, given the correspondence between 46050 U_w and AWAC U_w (Figure 2; Appendix), it was unlikely that spatial variability of the large-scale wave climate or bathymetry-induced changes in the local wave climate contributed significantly to the departures from theory. It appears much more

likely that temporal changes in forcing conditions (wind and waves), as well as a bathymetry-induced breakdown of the two-dimensional (2D) assumption used, contributed heavily to the observed variability. Important instances of both contributions are highlighted below.

The increase in regression slopes found after day 190 was coherent across the array, inferring that a region-wide change in wave or wind forcing affected the correspondence between observations and theory. Indeed, fluctuations of U_{obs} were visually larger than U_w at stations LB, LBS, and YB, and similar in magnitude as U_w at stations SR and SH (Figure 2), both in contrast with early season observations. The reason for this change remains puzzling. While the general wave direction shifted to be more northwesterly in origin (positive incoming direction; Figure 3) during this period, the addition of wave direction did not significantly effect the estimate of U_w (AWAC U_w; Figure 2). Based on nearby hydrographic observations made by PISCO, the vertical structure of the water column changed from more stratified conditions during the fluctuating wind forcing occurring early in the season to weakly stratified conditions as sustained upwelling winds took hold after day 190. It is tempting to infer that these changes in wind forcing and stratification were somehow responsible for the increased regression slopes observed, but a mechanism has yet to be identified.

Complex bathymetry existed around and onshore of many of these stations (Kirincich et al. 2005), in contrast to the smooth sandy beach sites used by Lentz et al. (2008), thus some degree of bathymetry-induced departure from the 2D assumptions of the theory could be expected. It was apparent from the depth-averaged mean velocities (Figure 2) and regression slopes (Table 1) that this assumption can break down at individual stations or over shorter spatial scales. Stations LB and LBS, located 1 km apart, have large differences in both mean across-shelf velocities (0.005 m and -0.01 m s^{-1} respectively) and regression slopes

between U_{obs} and U_w (0.59±0.3 and 2.2±1.3 respectively). In contrast, U_{obs} was consistently smaller than U_w at both SH and SHN, also separated by 1 km. The differences from theory seen at these stations could be due to control of the depth-averaged velocities by along-shelf variations in bathymetry.

Despite these variable individual results, the average over both space and time approached the 2D results found by Lentz et al. (2008). Because of this correspondence, we hypothesize that these sources of variability can be considered noise around the 2D result. The inclusion of more observations from additional stations or longer deployments would lead to a clearer result.

The inferred wave-driven, across-shelf velocity profiles (Figure 5), while different from the theoretical prediction, were similar both in magnitude and shear to the 'summer' profiles described by Lentz et al. (2008). Obtained in a water depth of 12 m during times of minimal wind forcing, this mean summer profile (shown in their Figure 12) had near zero across-shelf velocities in the bottom half of the water column and offshore flows in the top half, reaching a peak value just below the top of the measured portion of the water column. Similar to what was observed here, both the peak magnitudes and vertical shear of the Lentz et al. (2008) summer profile were stronger in the top half of the water column than that predicted by the theoretical model. Near-surface velocities were similarly reduced in magnitude relative to the peak velocity. In contrast, during winter when waters were more unstratified, the mean across-shelf velocity profile closely matched the theoretical prediction (Lentz et al. 2008). Stratification is generally stronger during summer at both locations sampled by Lentz et al. (2008) as well as the Oregon coast, perhaps serving as a link between the vertical structures found and their disagreement with the theoretical profiles. However, the current theoretical

understanding for wave-driven return flow due to the Hasselmann wave stress is independent of stratification. Thus it is not known how increased stratification would cause the differences seen between these summer profiles and linear theory.

Our re-examination of across-shelf exchange due to along-shelf wind forcing found that subtracting estimates of the wave-driven return flow from the observed across-shelf velocities had no significant effect on the mean fraction of full Ekman transport present at water depths of 15 m. The similarities between the observed and differenced profiles during all but moderate to strong downwelling events using the u_{obs}-u_{ap} profile indicates that the vertical structure of the wind-driven component of the across-shelf circulation was generally much larger than the vertical structure of the wave-driven component. Thus, it is unlikely that the Ekman fractions reported by Kirincich et al. (2005), obtained from similar observations in similar water depths, were significantly affected by wave-driven circulation. These results contrast with that seen by Fewings et al. (2008) for across-shelf exchange driven by across-shelf wind stress at the Martha's Vineyard site used by Lentz et al. (2008). Fewings et al. (2008) found that the vertical structure of the wave-driven return flow was of the same magnitude as the wind-driven, across-shelf circulation, altering observations of across-shelf exchange during most wave climates and wind forcing conditions.

From our results, we infer that process studies of coastal areas with similar conditions as the Oregon inner-shelf (strong wind forcing and stratification) may be able to ignore the wave-driven circulation when examining across-shelf exchange due to upwelling winds at similar water depths. This is an important conclusion given the inherent difficulty in isolating the wave-driven flow. However, given conditions more similar to Fewings et al. (2008), including: shallower depths, stronger wave forcing, and perhaps even significant

downwelling; future studies may still need to resolve the wave-driven circulation to study wind-forced, across-shelf exchange. The vertical structure of wave-driven circulation would be larger in shallower water depths or for larger significant wave heights. Reduced inner-shelf stratification, which is though to occur during downwelling (Kirincich and Barth 2009; Austin and Lentz 2002), or weaker wind forcing would decrease the vertical structure of the wind-driven circulation relative to the wave-driven circulation. A number of these factors may have contributed to the larger u_{obs}-u_{ap} profiles seen here during downwelling.

Our inability to fully isolate the wave-driven transport from the wind-driven exchange using this dataset suggests that only much larger datasets, such as that used by Lentz et al. (2008), would be able to clearly realize the wave-driven transport. A process study with limited observations would be unable to resolve this circulation and need to account for the potential biases from wave-driven transport on their velocity observations using theoretical estimates. However, given the differences in magnitude and vertical structure between wave-driven, across-shelf velocity profiles based on linear theory and both the Lentz et al. (2008) summer profiles and those found here, additional work is needed to develop an accurate theoretical description of wave-driven circulation under these more stratified conditions. Finally, our work was unable to answer whether the wave-driven transport causes real across-shelf exchange in the inner shelf, as a wave-driven undertow would do within the surf-zone. A detailed study describing this process and its interactions with the complex dynamics of the inner shelf is necessary to address these outstanding questions and fully understand across-shelf exchange in this critical region between the nearshore and the coastal ocean.

6. Summary

This extension to the work of Lentz et al. (2008) has examined the wave-driven return flow due to the Hasselmann wave stress (the Stokes-Coriolis force) along the central Oregon inner-shelf. Observed depth-averaged, across-shelf velocities were generally correlated with theoretical estimates of the proposed return flow, yet substantial temporal and spatial variability existed. During times of minimal wind forcing, the inferred across-shelf, wave-driven velocity profiles were surface intensified and increased in magnitude with increased significant wave height. While these results were consistent with circulation due to the Hasselmann wave stress, the magnitude of the inferred wave-driven return flow was substantially greater than estimates based on linear wave theory and matched that found by Lentz et al. (2008) during summer. Yet, subtracting estimates of the wave-driven return flow from the observed across-shelf velocities had no significant effect on the fraction of full Ekman transport present. Thus the potential bias due to unresolved wave-driven return flow in these observations of across-shelf exchange due to along-shelf wind stress was small.

APPENDIX

Stokes transport simplifications

To assess the representativeness of the simplifications made to equation (1), we compared this 46050-based estimate of U_w to estimates based on the local wave observations made by the AWAC at stations SHN and LBS. Combining the results for both stations, the 46050-

derived estimate of U_w was highly correlated (0.94±0.13) with, and close in magnitude (regression slope = 1.01±0.03) to the AWAC-derived U_w estimated using (1) and including the non-zero incoming wave direction (Figure 3). For visual comparison, both timeseries of U_w are shown in Figure 2. Additionally, we assessed whether use of significant wave height in finding U_w, instead of the full wave height spectrum, had an affect on U_w by comparing 46050 U_w to the integral of $U_w(\omega)$, the onshore transport caused by the observed wave height spectrum in the frequency band 0.02-0.5 Hz. This estimate of U_w was also highly correlated with 46050 U_w, but had an increased regression slope (1.04±0.06). Going one step further, using the full frequency-directional spectrum for each AWAC-measured wave burst, we compared 46050 $u_H(z)$ calculated using (3) and assuming θ=0, to the double integral of $u_H(z, \omega, \theta)$, integrated over the full frequency-directional spectrum for the frequency band of 0.02-0.5 Hz and incoming wave directions from -90 to 90 degrees (south to north). The depth-averaged means of these timeseries had an equally high correlation but an increased regression slope (1.11±0.07). From these comparisons, we infer that the simplifications made to enable use of the buoy observations, assuming $\theta = 0$ and reducing 46050 H_{sig} by 0.78, have only a small effect: overestimating the transport (U_w) or the vertical profile of the theoretical wave-forced return flow ($u_H(z)$) by 10% or less. Thus the 46050-based wave observations are used at all stations in the analysis that follows, allowing the full inclusion of the four stations where local wave measurements were not available.

Acknowledgments.

This is contribution number 338 from PISCO, the Partnership for Interdisciplinary Studies of Coastal Oceans funded primarily by the Gordon and Betty Moore Foundation and David and Lucile Packard Foundation. We thank J. Lubchenco and B. Menge in establishing and maintaining the PISCO observational program at OSU as well as Captain P. York, C. Holmes, and S. Holmes for their data collection efforts, and W. Waldorf for his assistance designing the AWAC bottom lander. Additional instrumentation was provided by Nortek-AS through a 2005 Nortek Student Equipment Grant award to AK. SL acknowledges support from NSF Ocean Science grant #OCE-0548961. AK acknowledges support from the WHOI Coastal Ocean Institute Fellowship.

REFERENCES

Austin, J. and S. Lentz, 2002: The inner shelf response to wind-driven upwelling and downwelling. *J. Phys. Ocean.*, **32**, 2171.

Barth, J., et al., 2007: Delayed upwelling alters nearshore coastal ocean ecosystems in the northern California Current. *Proc. Nat. Acad. Sci.*, **104 (10)**, 3719–3724.

Chelton, D., 1983: Effects of sampling errors in statistical estimation. *Deep-Sea Res.*, **30**, 1083–1101.

Fewings, M., S. Lentz, and J. Fredericks, 2008: Observations of cross-shore flow driven by cross-shore winds on the inner continental shelf. *J. Phys. Oceans. (in press).*

Garrett, C. and B. Petrie, 1981: Dynamical aspects of the flow through the strait of Belle Isle. *J. Phys. Ocean.*, **11 (3)**, 376–393.

Hasselmann, K., 1970: Wave-driven inertial oscillations. *Geophy. Fluid Dyn.*, **1 (4)**, 463–502.

Huyer, A., 1983: Coastal upwelling in the California Current System. *Prog. Oceano.*, **12**, 259–284.

Kirincich, A. and J. Barth, 2009: Time-varying across-shelf Ekman transport and vertical eddy viscosity on the inner-shelf. *J. Phys. Ocean.*, **39**, 602–620.

Kirincich, A., J. Barth, B. Grantham, B. Menge, and J. Lubchenco, 2005: Wind-driven inner-shelf circulation off central Oregon during summer. *J. Geophys. Res.*, **110 (C10S03)**, doi:10.1029/2004JC002 611.

Large, W. and S. Pond, 1981: Open ocean momentum flux measurements in moderate to strong winds. *J. Phys. Ocean.*, **11**, 324–336.

Lentz, S., M. Fewings, P. Howd, J. Fredericks, and K. Hathaway, 2008: Observations of undertow over the inner continental shelf. *J. Phys. Oceans., (in press)*.

Lentz, S. and J. Trowbridge, 2001: A dynamical description of fall and winter mean current profiles over the northern California shelf. *J. Phys. Ocean.*, **31 (4)**, 914–931.

Madsen, O., 1978: Mass transport in deep-water waves. *J. Phys. Ocean.*, **8**, 1009–1015.

Monismith, S. and D. Fong, 2004: A note on the potential tranport of scalars and organisms by surface waves. *Limnol. Oceanogr.*, **49 (4)**, 1214–1217.

Mooers, C., 1968: A compilation of observations from moored current meters and thermographs, vol 2: Oregon continental shelf, August-September 1966. *OSU Data Report*, **(68-5)**.

Newberger, P. and J. Allen, 2007: Forcing a three-dimensional, hydrostatic, primitive-equation model for application in the surf zone: 2. application to duck94. *J. Geophys. Res.*, **112 (C08019)**, doi:1029/2006JC003 474.

Perrie, W., C. Tang, Y. Hu, and B. DeTracy, 2003: The impact of waves on surface currents. *J. Phys. Oceano.*, **33 (L22S04)**, 2126–2140.

Polton, J., D. Lewis, and S. Belcher, 2005: The role of wave-induced Coriolis-Stokes forcing on the wind-driven mixed layer. *J. Phys. Oceano.*, **35**, 444–457.

Rascle, N., F. Ardhuin, and E. Terray, 2006: Drift and mixing under the ocean surface: A coherent one-dimensional description with application to unstratified conditions. *J. Geophys. Res.*, **111 (C03016)**, doi:10.1029/2005JC003 004.

Reed, B., 1992: Linear least-squares fits with errors in both coordinates. *Am. J. Phys.*, **60 (1)**, 59–62.

Samelson, R., et al., 2002: Wind stress forcing of the Oregon coastal ocean during the 1999 upwelling season. *J. Geophys. Res.*, **107 (C5)**, doi: 10.1029/2001JC00 900.

Tilburg, C., 2003: Across-shelf transport on a continental shelf: do across-shelf winds matter? *J. Phys. Oceano.*, **33**, 2675–2688.

Ursell, F., 1950: On the theoretical form of ocean swell on a rotating earth. *Mon. Not. Roy. Atron. Soc., Geophys. Suppl.*, **6**, 1–8.

Weber, J., 1981: Ekman currents and mixing due to surface gravity waves. *J. Phys. Oceano.*, **11**, 1431–1435.

Weber, J., 1983: Steady wind- and wave-induced currents in the open ocean. *J. Phys. Oceano.*, **13**, 524–530.

Weber, J., 2003: Wave-induced mass transport in the oceanic surface layer. *J. Phys. Oceano.*, **33**, 2527–2533.

List of Figures

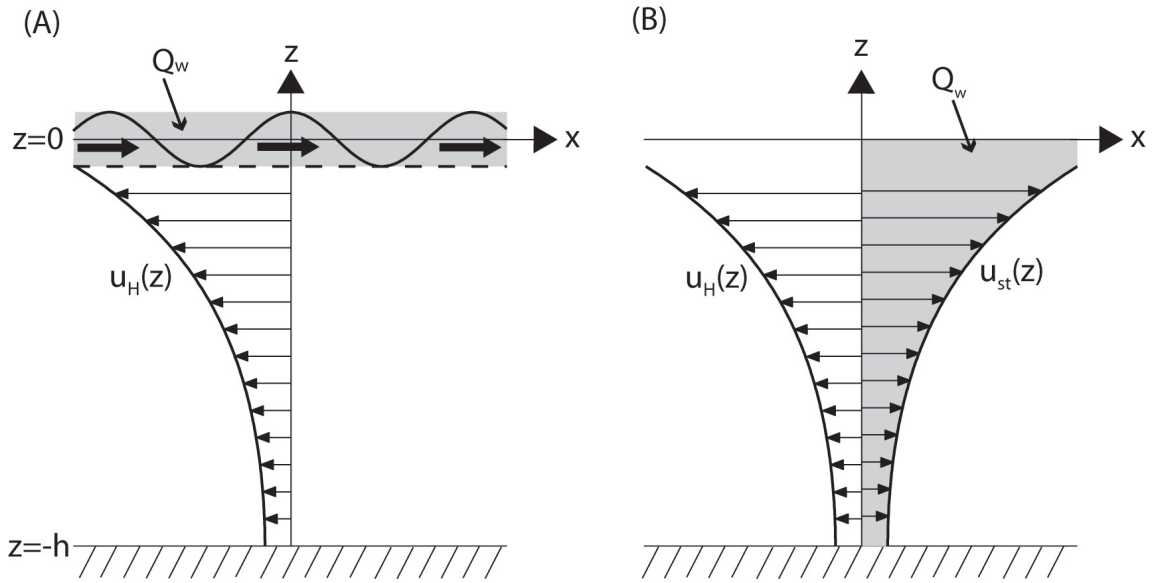

FIG. 1. Wave-driven circulation in an **(A)** Eulerian and **(B)** Lagrangian reference frame, following Fewings et al. (2008). The net, wave-averaged, onshore mass transport (Q_w) occurs only above the wave troughs in the Eulerian reference frame, but is distributed throughout the water column in the Lagrangian reference frame as Stokes drift (u_{st}). Regardless of the reference frame, outside of the surfzone this onshore mass transport is hypothesized to be balanced by the Hasselmann wave stress (the Stokes-Coriolis force) distributed as (u_H).

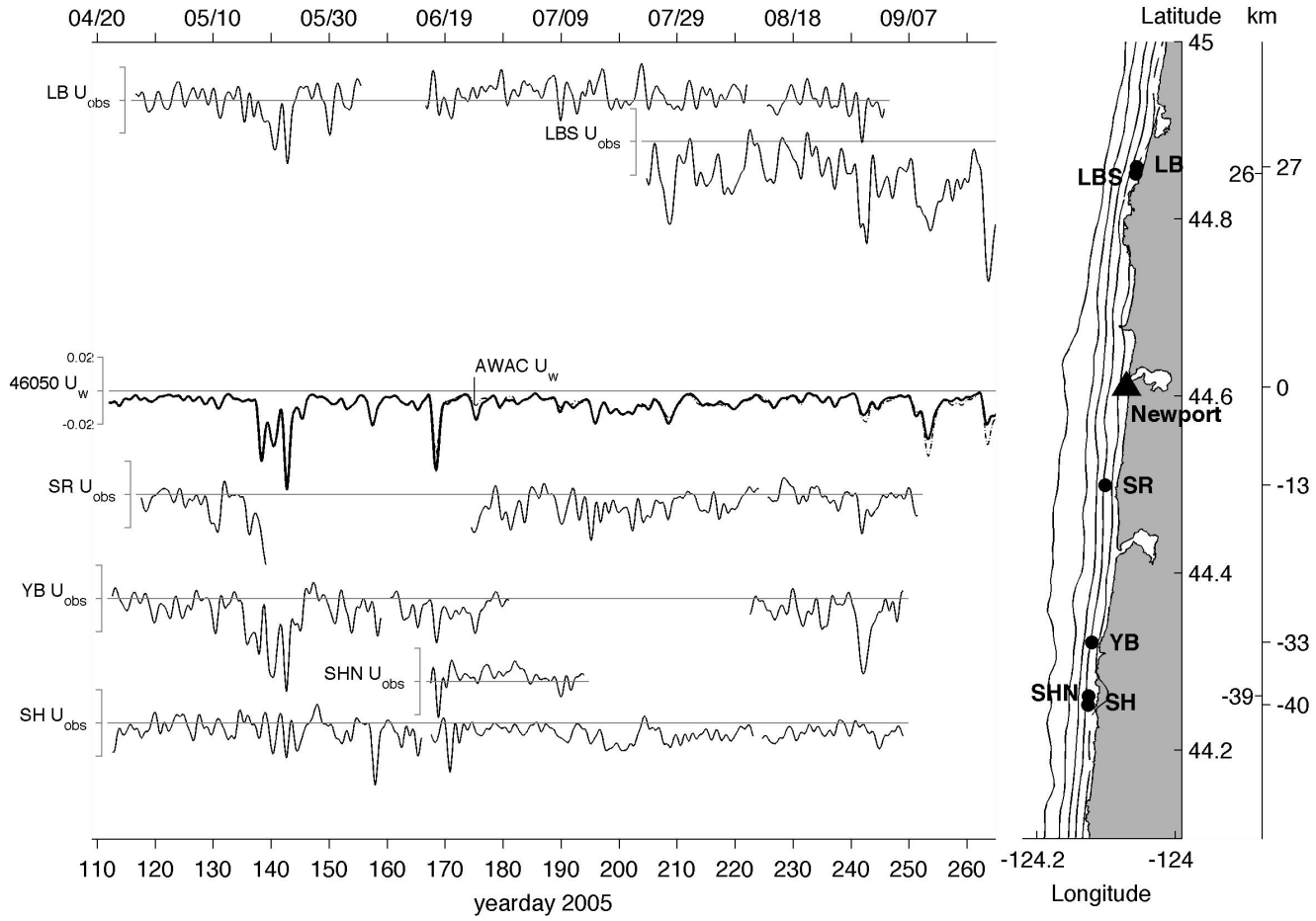

FIG. 2. At right, a map of the central Oregon inner shelf shows the locations of the six inner-shelf stations *(bullets)* and the Newport wind station *(triangle)*. Bathymetry contours are shown in 10 m increments for waterdepths of 50 m or less. At left, low-pass filtered timeseries of observed depth-averaged across-shelf velocity (U_{obs}) at each site are shown in their relative along-shelf locations. Vertical tick marks at the left of each timeseries denote ± 0.02 m s^{-1}. Additionally, timeseries of wave-driven return flow predicted from buoy 46050 wave observations (*solid*, 46050 U_w) and from AWAC wave observations (*dashed*, AWAC U_w), which include wave direction, at SHN (days 166-194) and LBS (days 203-265) are shown at the approximate latitude of buoy 46050 (44.6°). Buoy 46050 is located 33 km directly west of Newport.

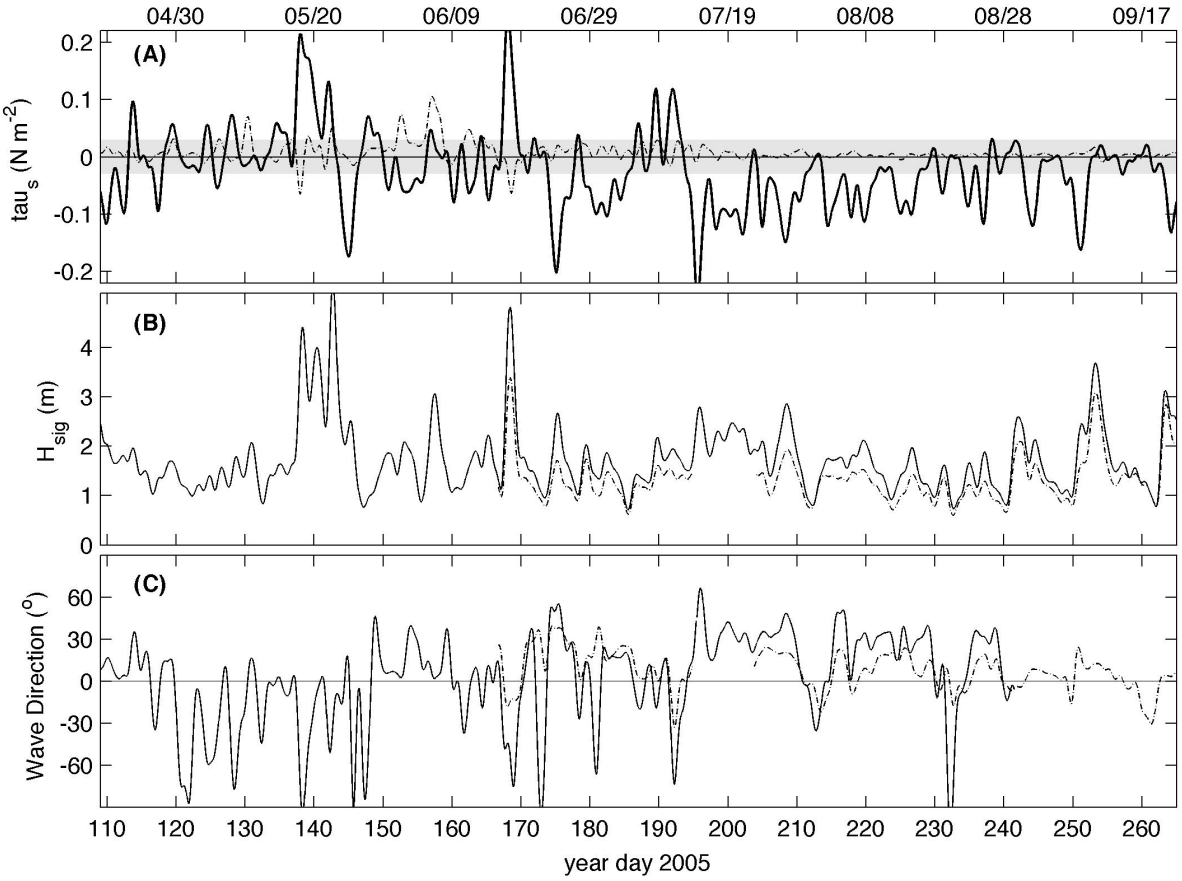

FIG. 3. Central Oregon coast conditions during the 2005 upwelling season: **(A)** Along-shelf *(solid)* and across-shelf *(dashed)* wind stress at Station NWPO3 in Newport. Wind stresses within the shaded region are less than ± 0.03 N m^{-2}. **(B)** Significant wave heights 33 km offshore of Newport at NDBC buoy 46050 *(solid)* and during the AWAC deployments *(dashed)* at stations SHN (days 166-194) and LBS (days 203-265). **(C)** Incoming wave direction from buoy 46089 (*solid*) and from the AWAC deployments (*dashed*) relative to 'shore normal' at the AWAC stations (defined as 270° at SHN before day 200 and 292° at LBS after day 200). All timeseries were low-pass filtered (40 hr half power period) to isolate the subtidal components of variability.

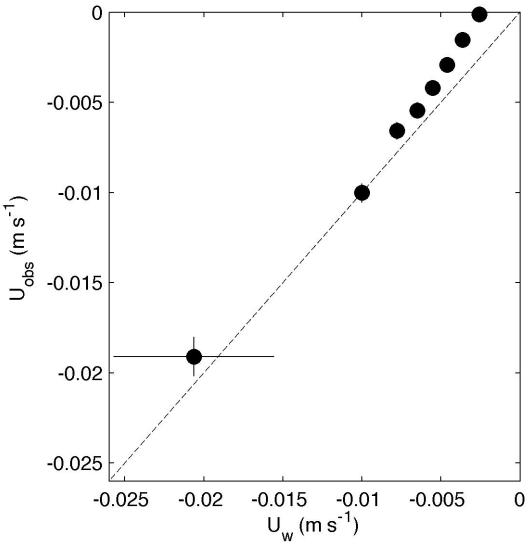

FIG. 4. Depth-averaged across-shelf theoretical return flow (U_w) verses observed (U_{obs}) velocities for all stations, all times. Circles mark the mean locations for each equal sample size (n=1586) bin, with standard error bounds in each direction. An exact match between the two timeseries would fall on the dashed line shown.

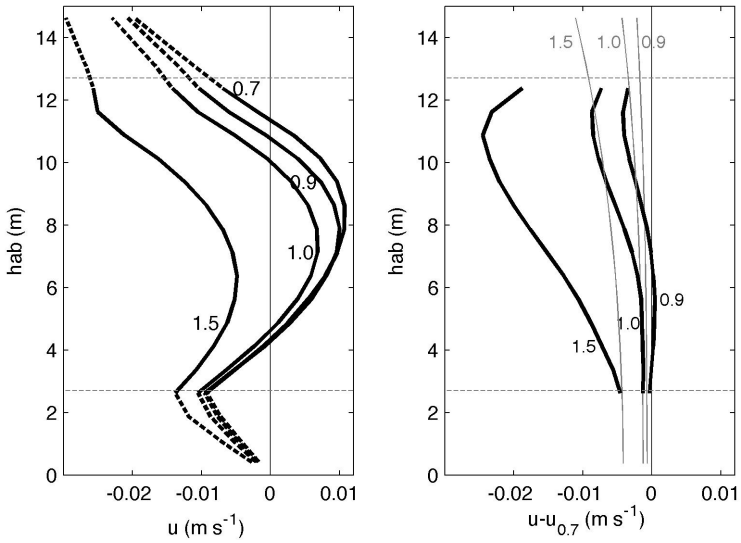

FIG. 5. **(Left)** Bin mean vertical profiles of across-shelf (u) velocity during minimal wind forcing and varying levels of H_{sig}/h. The mean H_{sig} (in m) for each equal sample-size (n=1192) bin is shown adjacent to each profile. Dashed lines mark the transitions from measured to extrapolated velocity profiles. **(Right)** The difference between the velocity profiles in the top three bins and that of the minimal-wind, minimal-wave profile ($u_{0.7}$) for both observations (*bold*) and theory (*grey*). The theoretical wave-driven, across-shelf return flow, calculated using (6), becomes increasingly negative with increasing H_{sig}.

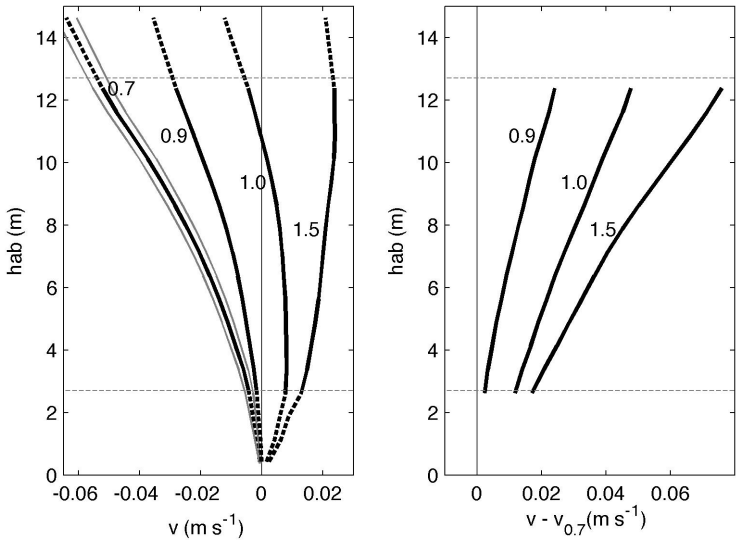

FIG. 6. **(Left)** Bin mean vertical profiles of along-shelf (v) velocity during minimal wind forcing and varying levels of H_{sig}/h. The mean H_{sig} (in m) for each equal sample-size (n=1192) bin is shown adjacent to each profile. Dashed lines mark the transitions from measured to extrapolated velocity profiles. Grey profiles bounding the $v_{0.7}$ m bin profile show the standard error bounds of this profile. Similar size bounds exist for the remaining profiles. **(Right)** Velocity differences (*bold*) between the bin mean across-shelf velocity profiles and the minimal-wind, minimal-wave profile ($v_{0.7}$).

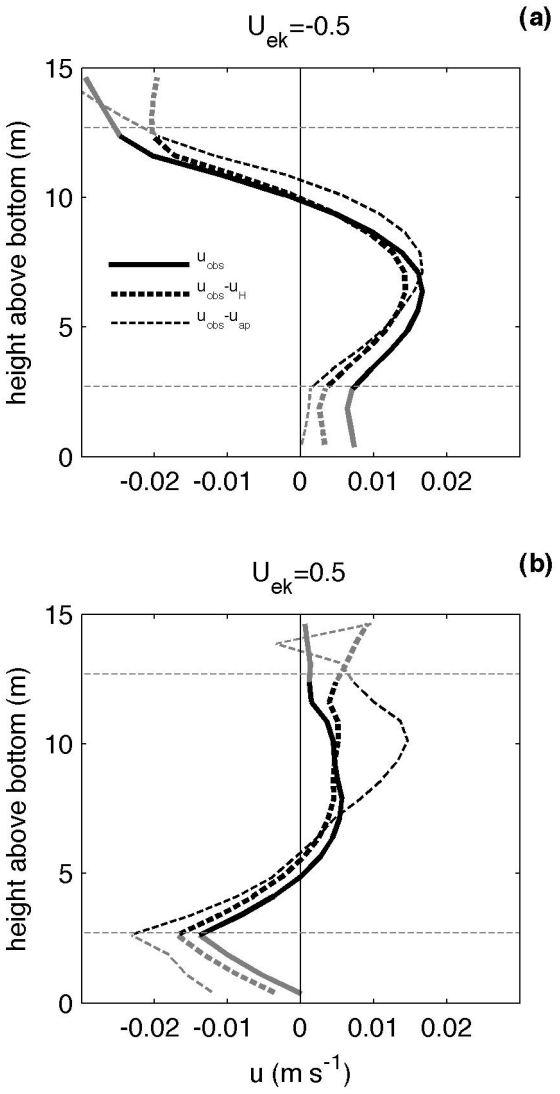

FIG. 7. Depth-dependent velocities for u_{obs} (*solid*), u_{obs}-u_H (*thick dashed*), and u_{obs}-u_{ap} (*thin dashed*) for **(a)** offshore, upwelling-favorable Ekman transport (U_{ek}=-0.5 m^3 s^{-1}) and **(b)** onshore, downwelling-favorable Ekman transport (U_{ek}=0.5 m^3 s^{-1}). Ekman transport was estimated as $U_{ek}=\tau_s^y/\rho f$, using the along-shelf wind stress, and profiles were averaged over a 0.1 m^3 s^{-1} window centered on $U_{ek}=\pm$0.5 m^3 s^{-1} before removing the depth-averaged mean to highlight across-shelf exchange. Grey shading and horizontal dashed lines denote the surface and bottom areas of extrapolation or interpolation. Mean significant wave heights for this level of wind stress were 1.3 m for upwelling and 1.4 m for downwelling (Figure 8).

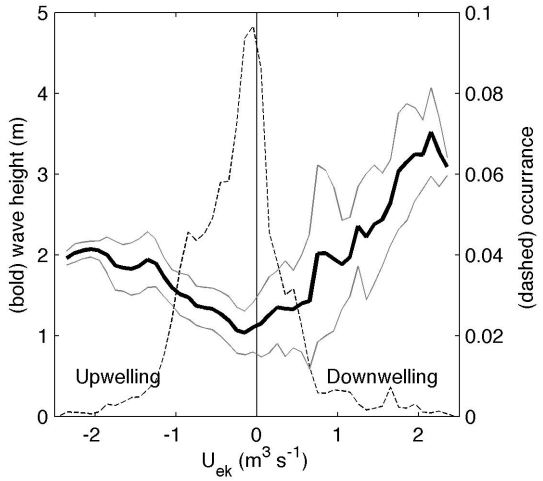

FIG. 8. Mean (*bold*) and standard deviation (*grey*) of significant wave height (H_{sig}) for varying levels of across-shelf Ekman transport (U_{ek}) due to the along-shelf wind stress. A histogram (*dashed*) of U_{ek} shows the dominance of negative, offshore theoretical transport, caused by upwelling-favorable, along-shelf winds.

List of Tables

TABLE 1. Correlation coefficients and regression slopes between observed depth-averaged across-shelf velocities (U_{obs}) and the theoretical depth-averaged return flow (U_w).

Station	Period (year days)									
	110-150		150-190		190-230		230-270		All	
	cc	slope	cc	slope	cc	slope	cc	slope	cc	slope
LB	**0.74**[a]	0.75±0.61	*0.07*		*0.17*		*0.59*		**0.46**	0.59±0.30
LBS	–		–		**0.84**	2.45±2.92	**0.80**	2.10±1.59	**0.78**	2.20±1.32
SR	**0.65**[c]	0.95±0.90	*0.68*		**0.54**	1.07±1.04	**0.81**	1.44±0.94	**0.62**[c]	1.08±0.51
YB	**0.75**	1.02±1.05	**0.58**[b]	0.54±0.35	*0.75*		**0.73**	2.75±2.26	**0.65**	0.90±0.41
SHN	–		**0.49**	0.35±0.30	*0.74*		–		**0.48**	0.35±0.28
SH	**0.39**[b]	0.25±0.23	*0.32*		**0.42**	0.51±0.48	*0.16*		**0.32**[b]	0.27±0.16
All	**0.60**[b,c]	0.67±0.36	**0.31**[b,c]	0.39±0.23	**0.47**	1.29±0.67	**0.57**	1.74±0.80	**0.45**[b,c]	0.80±0.22

[a]Statistically significant correlations are shown in **bold**.

[b]For this period, the difference between U_{obs} and U_w (U_{res}) was positively correlated with the along-shelf wind stress.

[c]For this period, the difference between U_{obs} and U_w (U_{res}) was negatively correlated with the across-shelf wind stress.

TABLE 2. Ekman transport fraction results.

station	Profile[a]					
	u_{obs}		u_{obs}-u_H		u_{obs}-u_{ap}	
	cc	fraction	cc	fraction	cc	fraction
LB	*0.12*		*0.12*		**0.23**	0.19±0.04
LBS	*-0.37*		*-0.48*		*-0.40*	
SR	**0.63**[b]	0.21±0.05	**0.62**	0.20±0.05	**0.66**	0.21±0.05
YB	**0.42**	0.22±0.08	**0.47**	0.21±0.07	**0.57**	0.22±0.08
SHN	**0.52**	0.18±0.07	**0.58**	0.18±0.08	**0.63**	0.18±0.08
SH	**0.43**	0.17±0.03	**0.44**	0.16±0.03	**0.52**	0.17±0.04

[a]See text for profile descriptions.

[b]Statistically significant correlations are shown in **bold**.